Pergamon

Int. J. Heat Mass Transfer. Vol. 39, No. 16, pp. 3475–3482, 1996

0017–9310/96 $15.00+0.00

PII: S0017–9310(96)00018–X

Holographic study of suspended vaporizing volatile liquid droplets in still air

G. R. TOKER and J. STRICKER†

Faculty of Aerospace Engineering, Technion—Israel Institute of Technology, Haifa 32000, Israel

(*Received* 29 *July* 1994 *and in final form* 23 *October* 1995)

Abstract—The data presented here describe the dynamics of vaporization of a single suspended droplet of chloroform, acetone and diethyl ether at room temperature and pressure in still air. The dual hologram technique was applied for direct measurements of the radial distribution of the change in the refractive index caused by the vapor molecules, Δn, in the vicinity of the vaporizing volatile liquid droplets as a function of time and droplet size. Δn was found to be a function of the similar dimensionless variable r/a where a is the droplet radius. Δn drops exponentially and exhibits an effect of free convection. In addition, it was found for all three substances that b, the radial distance at which the abrupt vapor concentration decrease occurs, is independent of drop size, i.e. the boundary of convection does not change in time. The reduction of interferometric data made it possible to determine saturation pressures, vapor densities and temperatures at the droplet surface. The variation of vapor density versus the dimensionless variable r/a was obtained from the interferometric measurements by assuming a theoretical temperature distribution. The vaporizing rate constants, K, and internal droplet temperatures T_i were measured at conditions where intensive heat transfer through the suspending fiber and thermocouple took place.

1. INTRODUCTION

Evaporation of a single isolated droplet in stagnant surrounding gas has been extensively studied both experimentally and theoretically, as reviewed in refs. [1, 2]. Different numerical models have been developed for investigation of this subject including the problem of droplet evaporation in a convective gas field [3, 4] and the influence of the fluid turbulence [5].

The different experimental approaches, which have been applied to study the process of evaporation of a single suspended droplet in still gaseous atmosphere, are discussed in detail in ref. [6]. The literature survey shows that there is essentially no mention of a study on vaporization of an isolated suspended droplet by optical techniques based on holography, in contrast with the extensive study of vaporization and burning of sprays by this method [7–11]. Also it is interesting to note that almost all the experimental results reported before were obtained for liquids of relatively low vapor pressures and no works have been done on volatile liquid droplets.

It is the objective of this paper to apply a new experimental approach of holographic interferometry for optical diagnostics of 'large' volatile liquid droplets, with diameters of the order of 2 mm, vaporizing in still air. In this paper the dual hologram technique is used to precisely measure the change of refractive index caused by vaporization. The influence of free convection on droplet vaporization is studied as well.

There are some difficulties in studying the vaporization process of relative small-size (radius of 1 mm and less) suspended liquid droplets by standard optical techniques. The main reasons are as follows. First, the diagnostic technique has to be able to provide high spatial resolution (<0.05 mm). Secondly, it has to be sensitive enough to measure the vapor density far away (a few droplet radii) from the surface of the droplet, bearing in mind that a low-concentration vapor density decreases fast, the coefficient of refractivity for a separate vapor molecule $C_v = (n_v^0 - 1)/N_0$ is very low, smaller than 4×10^{-23} cm^3, and the optical path is very short. n_v^0 is index of refraction of the vapor at normal conditions, and N_0 is the Loschmidt number. The dual hologram technique was chosen because of its high sensitivity and high spatial resolution.

2. EXPERIMENTAL

To successfully conduct interferometric experiments and obtain reliable phase information, special measures were taken.

First, chloroform, acetone and diethyl ether (in the order of rising volatility) highly volatile liquids, were chosen because of the high refractive coefficients of their vapors ($n_{ch}^0 = 1.00145$; $n_{ac}^0 = 1.00109$; $n_{de}^0 = 1.00153$).

Second, relatively large droplets with initial diameters between 2000 and 3000 μm were studied to increase the optical path in the air–vapor mixture.

† Author to whom correspondence should be addressed.

NOMENCLATURE

a	droplet radius
b	boundary of free convection
C_v	coefficient of refractivity of separate vapor molecule $C_v = (n_v^0 - 1)/N_0$
C_g	coefficient of refractivity of separate air molecule
g	acceleration due to gravity
Gr_g	Grashof number of air
I	intensity of light in interferometric pattern
k	Boltzman constant, 1.38×10^{-16} erg[K^{-1}]
K	evaporation rate constant
M_v	molecular weight of vapor
n	refraction index
n_v^0	refraction index of vapor at normal conditions
N_v	vapor molecule density
N_A	Avogadro number, 6.023×10^{23} mol cm^{-3}
N_0	Loschmidt number, 2.687×10^{19} cm^{-3}
N_∞	surrounding air molecular density, 2.504×10^{19} cm^{-3}
P_v	partial vapor pressure
P_0	normal pressure, 760 mm Hg
P_∞	surrounding air pressure, 760 mm Hg
r	radius
S	phase shift
Sc	Schmidt number
Sh_g	Sherwood number of air
t	time
T	temperature
T_0	normal temperature, 273 K
T_∞	surrounding air temperature, 293 K
x, y, z	coordinates.

Greek symbols

δ	angle
Δ	change of parameter
ϕ	phase of a light wave
λ	wavelength of diagnostic beam
ν	kinematic viscosity of air
ρ_v	vapor mass density
ξ	dimensionless variable, r/a.

Subscripts

a	at the droplet surface
ac	acetone
b	at the free convection boundary
ch	chloroform
de	diethyl ether
g	gas phase (air)
s	saturated
v	vapor
va	vapor parameters at the droplet surface
0	normal conditions
∞	surrounding air condition.

Third, if the droplet is highly volatile it cools as it vaporizes because of loss of latent heat. Being cooler than the surrounding air, it absorbs heat by conduction through the suspending fiber and directly through the droplet surface [12]. The temperature depression, when the steady state is reached, and hence the partial pressure of the vapor on the surface of the droplet are dependent on the heat influx through the fiber. In order to increase the temperature of the droplet, and therefore the vapor density, a stainless steel fiber (small tube with 350 μm i.d. and 550 μm o.d.) with high thermal conductivity was used for suspending the droplet.

The volume temperature of the droplet T_i was measured by a thermocouple which was inserted into the droplet.

A second series of experiments was performed with the drops suspended from a tip of a calibrated thermocouple of o.d. of 500 μm.

As a source of coherent radiation, continuous wave He–Ne and argon ion lasers were used, with wavelengths 632.8 and 514.5 nm, respectively.

Dual hologram interferometry

It is well known that holographic interferometry has considerable advantages over classic interferometry. The major feature of holography lies in the ability to 'store' one or more optical waves propagated through the vapor under investigation. The 'stored' waves can then be analyzed through comparison with a 'reference' wave or with each other at different places and times [13]. The dual hologram approach, [14, 15], unlike the classic technique, makes it possible to reconstruct an interferometric picture with compensation for the aberrations of the optical systems. This feature leads to high sensitivity and hence to high accuracy [16], which is very important in the case of weakly-refracting phase objects like vapor around vaporizing liquid droplets.

The dual hologram method allows to measure reliably a fringe shift of 1/20. For a vaporizing droplet with a typical optical length of the order of $\sim\lambda$, this means an accuracy of $\sim 5\%$.

The dual hologram technique was applied to quantitatively study the change of the refractive index caused by the vapor molecules around the droplet. The unique feature of this technique is that the no-droplet and vaporizing conditions (object waves) are recorded at different times on separate holograms. The images are interfered upon reconstruction, and the fringe configuration is controlled by precisely

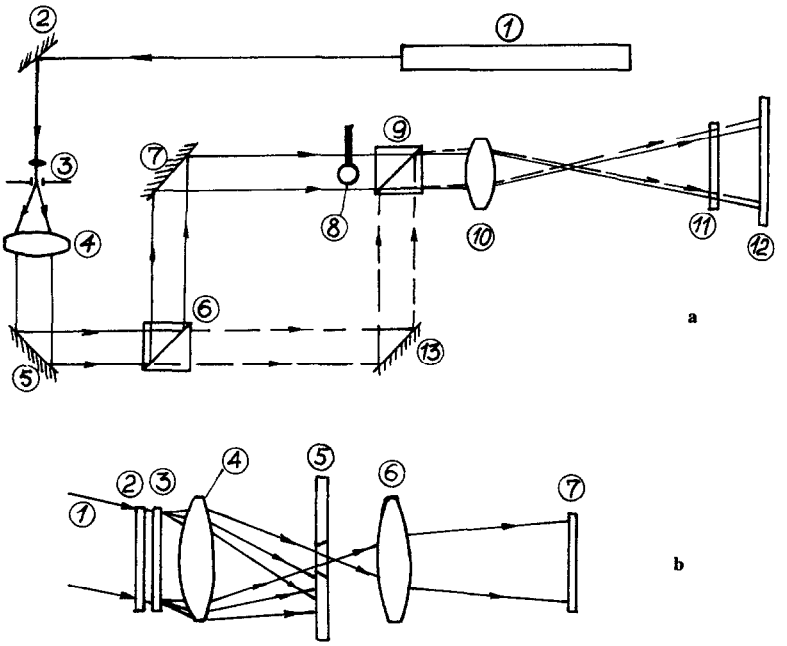

Fig. 1. Experimental set up. (a) Optical scheme for recording phase information. 1—continuous wave laser; 2, 5, 7, 13—100% Al-coated flat mirrors: 3—spatial filter (microobjective + pinhole); 4, 10 camera lenses; 6, 9—beam splitting cubes; 8—suspended droplet; 11—neutral optical filter; 12—hologram. (b) Optical scheme for reconstruction. 1—reconstructing laser beam; 2—object (droplet in) hologram; 3—reference (droplet out) hologram; 4—doublet achromat lens; 5—diaphragm; 6—camera lens; 7—reconstructed interferogram.

varying the orientation of the two holograms with respect to each other. This capability permits the formation of interferograms with any desired background fringe spacing and orientation, in particular perpendicular to the suspending fiber.

A classic Mach–Zehnder scheme, shown in Fig. 1(a), was used for making low spatial frequency 20–50 lines mm^{-1} holograms on AGFAPAN APX 25 and MIKRAT-200 films. The standard off-axis hologram recording technique was used, with an angle of less than 1° between the object and reference beams [17]. The spatial frequency of the holograms 12, was controlled by rotating the beam-splitting cube, 9.

The optical set up for reconstruction is shown in Fig. 1(b). The two object waves with and without the droplet are reconstructed in the +first order by simultaneously illuminating, 1, both holograms, 2, 3, as shown in Fig. 1(b). Other orders are stopped by a diaphragm, 5, placed in the focal plane of a doublet achromatic lens, 4. The focused image of the droplet is formed by the imagining camera lens, 6, on a photographic film, 7. A typical interferogram, with fringes perpendicular to the suspending fiber is shown in Fig. 2.

The dynamics of vaporization was investigated by holographing the droplet on film with a minimal time interval between frames of 6 s. The holograms were reconstructed yielding a series of interferograms. Each interferogram was analyzed and used to determine the radial distribution of the change in refractive index and the droplet size.

3. COMPUTATIONAL DATA ANALYSIS

Radial distribution of the vapor–air mixture index of refraction

Interferometric techniques are integrated methods, i.e. the measured information is the integrated product along the light path through the droplet vapor. If the

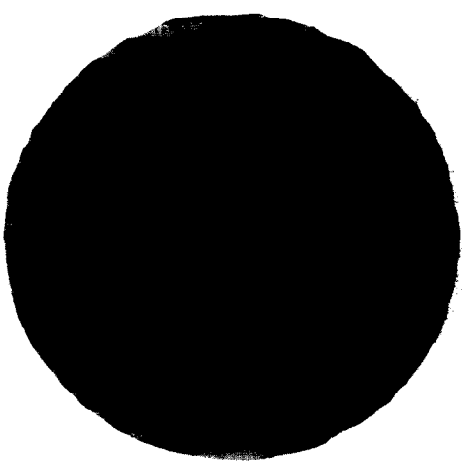

Fig. 2. Typical reconstructed interferogram of vaporizing chloroform droplet.

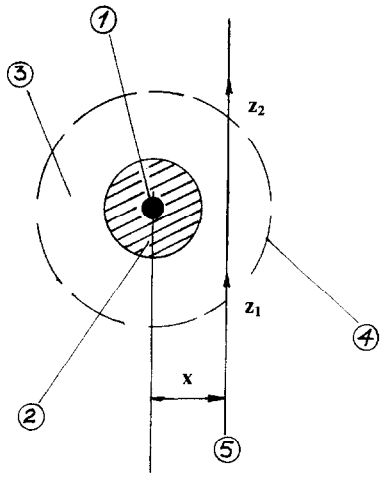

Fig. 3. Scheme of vaporizing drop dignostics. Top view. 1—suspending fiber; 2—droplet; 3—vapor; 4—boundary of vapor; 5—diagnostic light ray.

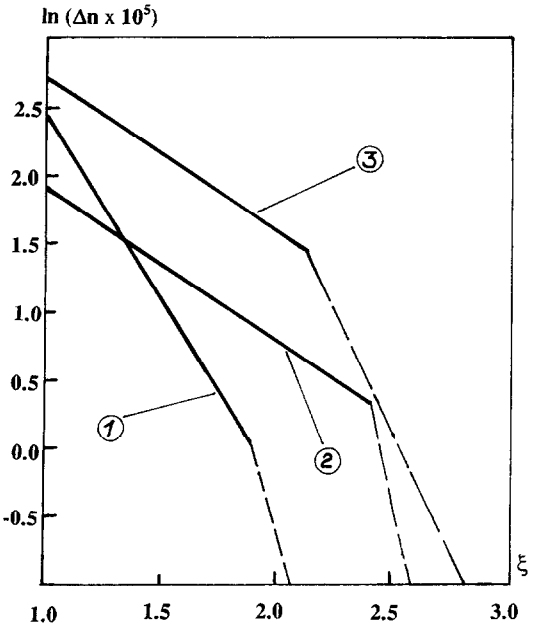

Fig. 4. Radial distribution of refractive index of droplet vapor vs dimensionless variable $\xi = r/a$. $\lambda = 632.8$ nm; $a = 930 \pm 20\mu$m. 1—chloroform; 2—acetone; 3—diethyl ether.

vapor around a droplet is probed by a collimated object beam (Fig. 3), the phase change $\Delta\phi(x, y)$ of the wave front, with the beam propagating in the z-direction is

$$\Delta\phi(x,y) = \frac{2\pi}{\lambda}\int_{z_1}^{z_2}[n(x,y,z) - n_\infty]\mathrm{d}z, \qquad (1)$$

where λ is the wavelength of the probing beam, $n(x, y, z)$ is the index refraction of the air–vapor mixture at point (x, y, z) and n_∞ is the index of refraction of the undisturbed air at room temperature and pressure. The irradiance in the reconstructed interferometric picture is modulated by the phase object as

$$I(x,y) \approx 1 + \cos\left[2\pi\frac{\sin\delta}{\lambda}y + \Delta\phi(x,y)\right], \qquad (2)$$

where δ is the angle between the reconstructed interfering waves and $\sin\delta/\lambda$ is the spatial frequency of the finite-width background interferometric fringes.

For the axisymmetric distribution of the vapor around the droplet (the fiber is the axis of symmetry) the relation (1) can be written in the form

$$S(x) = 2\int_x^R \frac{r\Delta n(r)}{(r^2 - x^2)^{1/2}}\mathrm{d}r, \quad a \leqslant r \leqslant R, \qquad (3)$$

where $S(x) = \Delta\phi/2\pi$, R is the extension of the phase object, r and x are independent geometric variables and $\Delta n(r) = n(r) - n_\infty$.

Since the function $\Delta n(r)$ is the desired quantity, the integral equation must be inverted. The inversion of equation (3), known as the Abel transform, is given by

$$\Delta n(r) = -\frac{\lambda}{\pi}\int_r^\infty \frac{\mathrm{d}S/\mathrm{d}x}{(x^2 - r^2)^{1/2}}\mathrm{d}x. \qquad (4)$$

In the analysis of interferometric data, the fringe order number $S(x)$ is obtained only at a finite number of discrete locations and therefore equation (4) must be solved numerically.

The solution of equation (4) yields the relationship $\Delta n = n(r) - n_\infty$ vs the radius r at various planes $y = \text{const}$. Such radial distributions of Δn were calculated for the equatorial cross-sections. The values of Δn were calculated with an accuracy of 10% for acetone and with a better accuracy for chloroform and diethyl ether because of their larger index of refraction. The radial distributions of $\Delta n(r)$ in the vicinity of the droplet surface, obtained for all three liquids with the wavelength $\lambda = 632.8$ nm, are shown in Fig. 4. Of the numerous reconstructed interferograms, those with droplet radii $a = 930 \pm 20$ μm were chosen for all three substances. The values $\Delta n = n(r) - n_\infty$ are plotted semi-logarithmically vs the dimensionless variable $\xi = r/a$.

A series of measurements using the wavelength $\lambda = 514.5$ nm was conducted for acetone droplets. The results for Δn measured around a certain droplet with radius changing with time are shown in Fig. 5. Note that the plots of $\ln(\Delta n)$ vs ξ are straight lines measuring that the index of refraction drops exponentially. The curves shown in Figs 4 and 5 enable us to determine the coefficients of refraction $(\Delta n)_a$, the vapor densities and saturation pressures very close to the droplet surface, as will be described in the following.

Determination of molecular vapor density, partial vapor pressure, and temperature on the droplet surface

Assuming that the droplet vaporizes at constant room pressure P_∞ into still air with known ambient

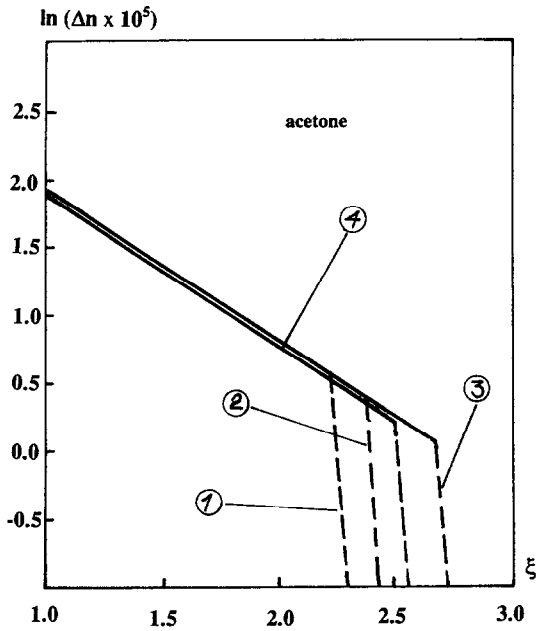

Fig. 5. Radial distribution of refractive index of acetone droplet vapor vs dimensionless variable $\xi = r/a$. $\lambda = 514.5$ nm. Droplet radii: 1—1160; 2—1090; 3—970 μm. $\lambda = 632.8$ nm. Droplet radius: 4—1030 μm.

temperature T_∞, the change of refractive index can be written in the form

$$\Delta n(x,y,z) = N_v(C_v - C_g) + N_\infty C_g(T_\infty/T - 1), \quad (5)$$

where T is the temperature of the air–vapor mixture and N_v is the molecular vapor density at the point (x,y,z). The second term on the right-hand side of this equation presents the change of the refractive index due to the cooling of the air-vapor mixture in the course of the vaporization. The molecular density N_v, pressure P_v, and the density ρ_v of the vapor can be evaluated from equation (5), taking into account the gas law $P = NkT$, as:

$$\frac{N_v}{N_\infty} = \frac{\Delta n}{N_\infty(C_v - C_g)} - \frac{C_g}{(C_v - c_g)}\left(\frac{T_\infty}{T} - 1\right), \quad (6)$$

$$\frac{P_v}{P_\infty} = \frac{T}{T_\infty}\left[\frac{\Delta n}{N_\infty(C_v - C_g)} - \frac{C_g}{C_v - C_g}\left(\frac{T_\infty}{T} - 1\right)\right], \quad (7)$$

$$\rho_v = M_v N_v / N_A, \quad (8)$$

where M_v is the molecular mass of a vapor and N_A is Avogadro number.

If one assumes that the partial vapor pressure at the droplet surface P_{va} is equal to the saturation pressure P_s which corresponds to the surface temperature T_a, the values P_{va} and T_a can be obtained by solving equations (7), together with the experimental dependence of the saturation pressure vs temperature [18]. The required coefficients of refraction $(\Delta n)_a$, close to the droplet surface, were determined from the plots of $\ln(\Delta n)$ vs r/a shown in Figs. 4 and 5. The partial pressures thus obtained are given in Table 1. The table includes the values of the vapor molecular density N_{va}, and the vapor mass density ρ_{va}, at the droplet surface, as obtained from equations (6) and (8), respectively. The calculated surface temperature T_a, and the volumetric measured temperature T_i, are given in the table as well.

Effect of free convection

A droplet being suspended in still air induces free convection as a result of the increase in the air density near the droplet, due to the surface temperature decrease. Free convection is characterized by the Grashof number

$$Gr = \frac{8r^3 g}{\nu^2}\frac{T_\infty - T_a}{T_\infty}.$$

The temperature of the droplet is weakly affected by free convection, but the rate of vaporization is increased by a factor equals to the Sherwood number [12]

$$Sh_g = 1 + 0.15 Sc^{1/3} Gr_g^{1/4},$$

Table 1. Parameters characterizing vaporization of suspended volatile liquid drops in still air at $T_\infty = 293$ K, $P_\infty = 760$ mm Hg

Drop suspended on stainless steel fiber

Substance	M, [g mol^{-1}]	T_i, [K]	T_a, [K]	P_{va}, [mm Hg]	N_{va}, [10^{19} cm^{-3}]	ρ_{va}, [10^{-3} g cm^{-3}]	K, [10^{-3} cm^2 s^{-1}]
Chloroform	119.4	275	274	63	0.22	0.44	1.2
Acetone	58.1	276	255	26	0.10	0.10	0.72
Diethyl ether	74.1	265	252	59	0.23	0.28	1.4

Drop suspended on thermocouple

Substance	T_i,[K]	K[10^{-3} cm^2 s^{-1}]
Chloroform	271	0.46
Acetone	272	0.31
Diethyl ether	261	0.64

Table 2. Grashof and Sherwood numbers for free convection of volatile liquid drops vaporizing in still air at $T_\infty = 293$ K, $P_\infty = 760$ mm Hg. The drops are suspended on stainless steel fiber

Substance	Radius [cm]	Gr_g	Sh_g
Chloroform	0.1	29	1.35
Acetone	0.1	37	1.37
Diethyl ether	0.1	44	1.39

where Sc is the Schmidt number. Typical free convection factors for the three substances are presented in Table 2. The high values obtained, indicate that a strong effect of free convection is expected.

The behavior of the plots in Figs. 4 and 5 for distances from the droplet surface above $(1.0–1.5) \times a$, confirms the fact that in nominally still air, free convection takes place. The air movement abruptly reduces the vapor concentration far from the droplet surface. It was found that for all three substances the radial distance, b, at which the abrupt density decrease occurs, is independent on drop size, i.e. the boundary of convection does not change in time. This indicates that the smaller droplets are less affected by free convection (see Fig. 5 for acetone).

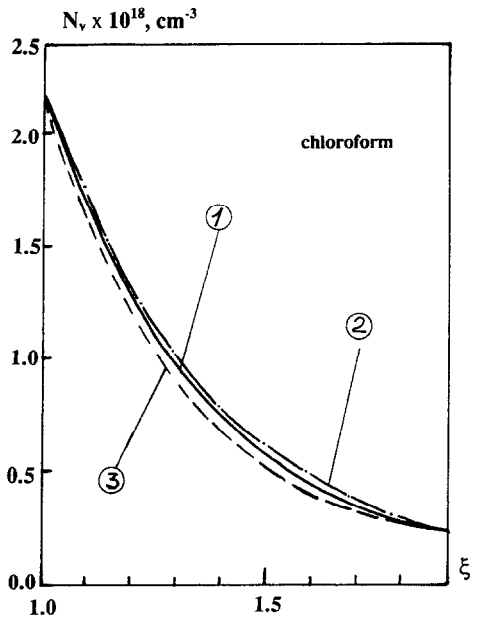

Fig. 6. Radial distribution of vapor density vs dimensionless variable $\xi = a/r$. Chloroform droplet. Droplet radius $a = 1030 \pm 20$ μm. Temperature distributions: 1—equation (9); 2—parabolic equation (10); 3—linear, equation (11).

Radial distribution of molecular vapor density

Equation (5) shows that the refractive index is a function of the vapor concentration and the temperature. These values were determined independently only on the droplet surface, as described in the previous section. However, from Δn vs r/a, obtained from the interferometric measurements, it is impossible to calculate the vapor density distribution without knowing the temperature distribution.

It is well known that the so-called 'two wavelengths' or the 'multicolor' techniques [19–21] had been applied successfully to measure the temperature and concentration fields separately. Unfortunately, in our case, the dispersive power of the vapor for the two wavelengths used is very small, therefore it is impossible to use this technique in the present experiment. This is seen in Fig. 5 where, within the limits of error, the curves for $\lambda = 632.8$ and 514.5 nm almost coincide.

In order to overcome the problem of the missing data required for the vapor density calculations, a theoretical temperature profile was used, given by [6]

$$\frac{T}{T_\infty} = \frac{T_a}{T_\infty} + \frac{b}{r}\frac{r-a}{b-a}\left(1 - \frac{T_a}{T_\infty}\right) \quad \text{for } a \leqslant r \leqslant b. \tag{9}$$

Equation (9) was developed for a spherically symmetric low volatile liquid droplet, located at the center of a spherical enclosure. The enclosure radius is b and its wall temperature is T_∞. It was assumed that the profile described by equation (9) is true also for a volatile droplet suspended in unbounded still air. For this case, the enclosure radius b is replaced by the boundary of the free convection, and the wall temperature by T_∞, the temperature of the undisturbed surrounding air.

Figures 6 and 7 show the vapor molecular density variations obtained from equations (6), (8) and (9).

In order to evaluate the significance of the results for N_v obtained by using equation (9), it is important to study the sensitivity of the results of the temperature profile. A sensitivity study has been done by using two additional temperaure profiles. One is a parabolic profile, given by

$$\frac{T}{T_\infty} = \left(\frac{T_a}{T_\infty} - 1\right)\left(\frac{r-b}{a-b}\right)^2 + 1, \tag{10}$$

and the second is a linear profile

$$\frac{T}{T_\infty} = \frac{T_a}{T_\infty} + \frac{r-a}{b-a}\left(1 - \frac{T_a}{T_\infty}\right). \tag{11}$$

The results calculated with the parabolic (10) and the linear (11) temperature profiles are also shown in Figs. 6 and 7.

Determination of the vaporizing rate constant, K

It was shown theoretically and experimentally [6] that, after the initial stage of vaporization, the square of the droplet diameter decreases linearly with time, according to the equation

$$\mathrm{d}(2a)/\mathrm{d}t = -K, \tag{12}$$

where K is defined as the vaporizing rate constant.

In the two series of experiments, namely the experiments with the droplets suspended from the fiber and

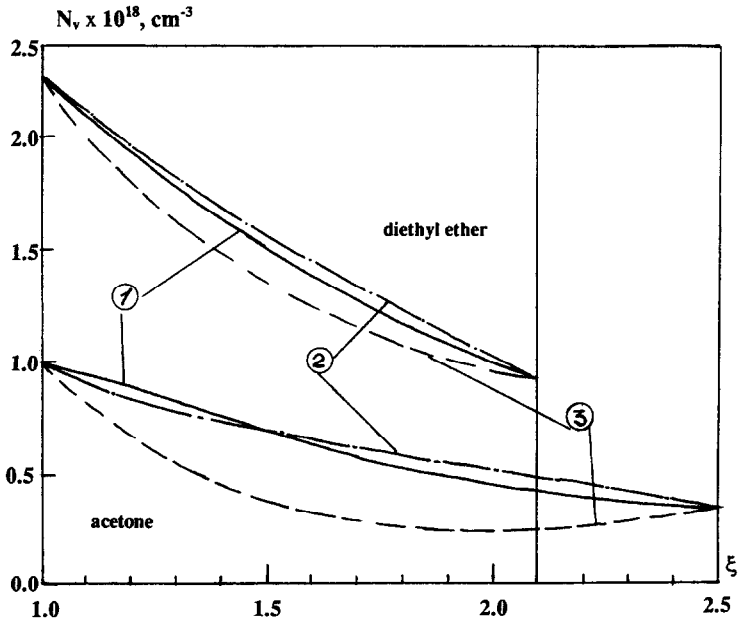

Fig. 7. Radial distribution of vapor density vs dimensionless variable $\xi = a/r$. Acetone and diethyl ether droplets. Droplet radii: 1030 ± 20 μm. Temperature distributions: 1—equation (9); 2—parabolic, equation (10); 3—linear, equation (11).

the experiments with the thermocouple, it was found that droplets vaporize in accordance with equation (12). The values of K were determined from the plots of the droplet diameter vs time. The results were obtained with accuracy of 5%, and are summarized in Table 1.

4. DISCUSSION

Figures 4 and 5 show that the refractive index around the droplets decrease exponentially with distance r/a. At distance $r > b$, an abrupt decrease in vapor density occurs due to the effect of free convection. It is observed that b, for each substance, is independent on droplet size.

The measured vaporizing rate constants, K, are summarized in Table 1. From the table it is seen that the measured values, K, for the droplets suspended on the steel fiber, are, respectively, higher than those measured for the droplets suspended on the thermocouple. These results indicate that the fiber conducts heat more rapidly to the drop, as compared with the thermocouple. The suspended droplet derives its energy from the surroundings both through the fiber (the thermocouple) and through the droplet surface. The rates of heat influx through the suspending fiber (thermocouple) and through the surface can be estimated by taking into account the measured rate constants K, the coefficient of the thermal conductivity of air and the geometrical sizes and thermal conductivities of the fiber and the thermocouple. These estimations show that the rate of heat influx through the fiber and thermocouple are approximately 200% and 50% of the heat influx through the surface, respectively. The temperature measurements by the thermocouple confirm these conclusions. Despite the fact that chloroform is a less volatile liquid than acetone, its measured vaporizing rate constant is significantly higher than that of acetone. This phenomena is consistent with the higher surface temperature obtained for chloroform $T_a = 274$ K relative to that of acetone $T_a = 255$ K. It also confirms the well known phenomena that the vaporization process depends mainly on the surface temperature.

The results obtained for T_a in the case of acetone and diethyl ether are considerably low compared with the respective temperature T_i measured by the thermocouple. The reason for the observed difference, $T_i - T_a$, is that for volatile liquid droplets the vaporization process remarkably lowers the temperature of the droplet surface. Similar results are reported in ref. [22], where it was shown that the difference $\Delta T = T_\infty - T_a$ becomes progressively larger with increasing volatility of the liquids. In the case of chloroform the surface temperature, T_a is approximately the same as the internal one, T_i. Why the difference $T_i - T_a$ is insignificant for the volatile chloroform is not clear.

Figure 6 shows that for the chloroform droplets the sensitivity of the density distribution to the temperature profile is very weak. The maximum difference between curves 1 and 2 is 6% and between curves 1 and 3 is 8%. These differences are within the limits of error of the experiment. In the case of acetone and diethyl ether droplets, see Fig. 7, the curves obtained with the linear temperature profile are significantly different from curve 1. The maximum difference is 50 and 15% for acetone and diethyl ether, respectively.

However, the curves 2 are close to curves 1, as for chloroform. Since it is reasonable to assume that the linear temperature variation is far from being real, we conclude that the present results of the vapor density variation are valid within a mean error of 10%.

5. SUMMARY

For the first time, holographic interferometry was applied to study the dynamics of vaporization of a suspended single droplet of acetone, chloroform and diethyl ether in unbounded, still air at room temperature and pressure. The main results of the present work are:

(1) The change of the refractive index around a vaporizing volatile droplet decreases exponentially with distance from the droplet surface and depends on the similar dimensionless variable $\xi = r/a$.

(2) The saturation pressures P_{va}, molecular densities N_{va}, mass densities ρ_{va} and temperatures T_a at the droplet surface were determined experimentally by means of reduction of interferometric data for all three substances.

(3) Free convection effects are important at $r > b$, where an abrupt decrease in vapor pressure occurs. It was observed that for a given substance, b is independent of the droplet size. $b \approx 2.0$; 2.6 and 2.2 mm for chloroform, acetone, and diethyl ether, respectively.

(4) Based on the assumptions that the actual temperature distribution is close to a spherically symmetric distribution of a low volatile droplet, the radial vapor density distributions were calculated for droplets with radii $a = 1030 \pm 20$ μm for all three substances. The validations of this assumption has been proven by sensitivity study to the temperature profile.

(5) Vaporizing rate constants K were experimentally obtained for all three substances, under conditions where the intensive heat influx was transferred to the droplet through the suspending fiber.

(6) In the case of acetone and diethyl ether, the surface temperatures T_a are considerably low compared with the volume temperatures T_i measured by a thermocouple. This effect is not observed with chloroform. The relatively high temperature at the surface of a chloroform droplet leads to the high measured value of vaporizing rate constant K_{ch}. The reason why there is no large difference between T_i and T_a in the case of chloroform is not clear.

REFERENCES

1. G. M. Faeth, Current status of droplet and liquid combustion, *Prog. Energy Combust. Sci.* **3,** 191–224 (1977).
2. W. A. Sirignano, Fuel droplet vaporization and spray combustion, *Prog. Energy Combust. Sci.* **9,** 291–322 (1983).
3. S. Prakash and W. A. Sirignano, Theory of convective droplet vaporization with unsteady heat transfer in the circulating liquid phase, *Int. J. Heat Mass Transfer* **23,** 253–268 (1980).
4. C. H. Chiang, M. S. Raju and W. A. Sirignano, Numerical analysis of convecting, vaporizing fuel droplet with variable properties, *Int. J. Heat Mass Transfer* **35,** 1307–1324 (1992).
5. A. Berlemont, M. S. Grancher and G. Gouesbet, On the Lagrangian simulation of turbulence influence on droplet evaporation, *Int. J. Heat Mass Transfer* **34,** 2805–2812 (1991).
6. N. A. Fuchs, *Evaporation and Droplet Growth in Gaseous Media*. Pergamon Press, Oxford (1959).
7. N. Chigier, Group combustion models and laser diagnostic methods in sprays: a review, *Combust. Flame* **51,** 121–139 (1983).
8. G. A. Ruff, L. P. Bernal and G. M. Faeth, High-speed in line holocinematography for dispersed-phase dynamics, *Appl. Opt.* **29,** 4544–4546 (1990).
9. F. Mayinger and A. Chavez, Measurements of direct-contact condensation of pure saturated vapor on an injection spray by applying pulsed laser holography, *Int. J. Heat Mass Transfer* **35,** 691–702 (1992).
10. N. Zhang, B. X. Wang and Y. Xu, Thermal instability of evaporating drops on a flat plate and its effect on evaporation rate, *Int. J. Heat Mass Transfer* **30,** 462–468 (1987).
11. M. M. El Wakil, Interferometry. In *Combustion Measurements. Modern Techniques and Instrument* (Edited by R. Goulard), Part II, Session 7. Academic Press, New York (1976).
12. C. N. Davies, Evaporation of airborne droplets. In *Fundementals of Aersol Science* (Edited by D. T. Shaw), Chap. 3. Wiley, New York (1978).
13. C. M. Vest, *Holographic Interferometry* (1st Edn), p. 311. Wiley, New York (1979).
14. R. J. Radrey and A. G, Havener, Application of dual hologram interferometry to wind tunnel testing, *AIAA J.* **11,** 1332–1333 (1973).
15. I. S. Zelikovich, A. M. Lyalikov and G. R. Toker, Visualization of acoustic waves in a dye solution by holographic interferometry, *Sov. Tech. Phys. Lett.* **14,** 213–214 (1988).
16. J. D. Trolinger, Application of generalized phase control during reconstruction to flow visualization holography, *Appl. Opt.* **18,** 766–774 (1979).
17. R. E. Brooks, Low angle holographic interferometry using TRI-X pan film, *Appl. Opt.* **6,** 1418–1419 (1967).
18. *Handbook of Chemistry and Physics* (54th Edn). CRC Press, Cleveland, OH (1973–1974).
19. M. M. El-Wakil, An interferometric technique for measuring binary diffusion coefficients, *J. Heat Mass Transfer* **91,** 259–265 (1969),
20. F. Mayinger and W. Panknin, Holography in heat and mass transfer, Parer IL3. In *Proceedings of Fifth International Heat Transfer Conference*, 3–7 September, Tokyo, Vol. 6, pp. 28–43. Japanese Society Of Mechanical Engineers (1974).
21. W. K. Witherow, D. Villers and G. Whitelaw, Methods to detect and measure gradients in fluids and materials processing. In *Proceedings of 6th International Symposium on Experimental Methods for Microgravity Materials Science*. pp. 33–37 (1994).
22. G. O. Langstroth, C. H. H. Diehl and E. J. Winhold, The evaporation of droplets in still air, *Can. J. Res. A.* **28,** 580–595 (1950).